JORDAN JOURNAL OF BIOLOGICAL SCIENCES

Jordan Journal of Biological Sciences

Journal homepage: www.jjbsci.com

# Folate-Targeted $Fe_2O_3$-5-Fluorouracil Nanoconjugates: Synthesis, Characterization, and *In-Vitro* Anticancer Evaluation

Chaithra Rudrappa.[1], Shaila G Sanjeevagol[2]., Jayappa Manjanna[3], Anitha N[1], G. T. Ramya[1], M. Meghana[1], Sarathkumar E[1], Prashanth S. J.[4] and G. J. Sathisha[1*]

[1]Department of Postgraduate Studies and Research in Biochemistry, Jnana Sahyadri, Kuvempu University, Shankaraghatta, Shivamogga- 577 451, Karnataka, India.
[2]Department of Chemistry, Sangolli Rayanna First Grade Constituent College. Belagavi-590017, Karnataka, India
[3]Department of Department of Chemistry, Rani Channamma University, Belagavi, 591156, Karnataka, India.
[4]Department of Postgraduate Studies and Research in Food Technology, Jnana Sahyadri, Kuvempu University, Shankaraghatta, Shivamogga- 577 451, Karnataka, India.

**To cite this article**: Chaithra Rudrappa, Shaila G Sanjeevagol, Jayappa Manjanna, Anitha N, G. T. Ramya, M. Meghana, Sarathkumar E, Prashanth S. J and G. J. Sathisha(2026) Folate-Targeted $Fe_2O_3$-5-Fluorouracil Nanoconjugates: Synthesis, Characterization, and In-Vitro Anticancer Evaluation; JJBS; 18:2, 46:54.

**Corresponding Author:**
**G. J. Sathisha**
Department of Postgraduate Studies and Research in Biochemistry, Jnana Sahyadri, Kuvempu University, Shankaraghatta, Shivamogga- 577 451, Karnataka, India
**Email:** satishlec@gmail.com

**ABSTRACT**

**Aim:** The aim of this study was to develop $Fe_2O_3$-based nanoconjugates (NCs) incorporating activated folic acid (FA) and 5-fluorouracil (5-FU) as a targeted system for delivering anticancer drugs and to evaluate their in-vitro efficacy.

**Background and Objective:** The clinical application of 5-FU in cancer therapy is limited by its short plasma half-life, nonspecific bio distribution, and dose-limiting systemic toxicity. Targeted-based drug delivery systems using nanocarriers offer a potential strategy to overcome these limitations. In this context, folic acid (FA) is a promising targeting ligand due to the overexpression of folate receptors in many cancer cells. The present study aimed to develop and evaluate a folic acid–mediated iron oxide nanoparticle (NP)-based delivery system for enhanced anticancer efficacy.

**Methods and Analysis:** $Fe_2O_3$ NPs were synthesized via a controlled precipitation-calcination method. FA was activated (AFA) using carbodiimide chemistry and conjugated with 5-FU, followed by surface functionalization onto $Fe_2O_3$ NPs. The obtained $Fe_2O_3$-AFA-5FU NCs were characterized using UV-visible spectroscopy, FTIR, and SEM. In-vitro biological evaluation was performed using MTT cytotoxicity assay, cell-cycle distribution analysis, caspase-3, -8, and -9 activity assays, and wound-healing migration assay.

**Results:** Spectroscopic and microscopic analyses confirmed the successful activation of AFA, its conjugation with 5-fluorouracil (AFA-5FU), and the subsequent surface functionalization of $Fe_2O_3$ NPs with AFA-5FU. The NCs shown significantly enhanced concentration-dependent cytotoxicity when compared with 5-FU, while $Fe_2O_3$ NPs showed favourable biocompatibility. Cell-cycle analysis revealed an increase in sub-$G_0/G_1$ population and $G_2$/M phase arrest. Caspase assays demonstrated dose-dependent activation of caspase-3, -8, and -9, indicating the involvement of both intrinsic and extrinsic apoptotic pathways. In addition, $Fe_2O_3$-AFA-5FU NCs significantly inhibited cell migration in wound-healing assays.

**Conclusion:** Collectively, folate receptor-mediated targeting and NP-assisted drug delivery improve intracellular drug accumulation and therapeutic performance, establishing $Fe_2O_3$-AFA-5FU NCs as a viable targeted cancer therapy platform.

**Keywords:** Lung cancer; A549 cells; $Fe_2O_3$ nanoparticles; Folic acid targeting; 5-Fluorouracil (5-FU); Targeted drug delivery; Nanocarriers; Anticancer therapy.

**ARTICLE HISTORY**

Received 20 Feb 2026
Accepted 25 Feb 2026

## 1. INTRODUCTION

Lung cancer continues to be a primary cause of cancer-related deaths globally, with non-small cell lung cancer (NSCLC) representing approximately 85% of all diagnosed instances (Molina et al., 2008). The A549 human lung adenocarcinoma cells were extensively used as an *in-vitro* NSCLC model owing to their well-defined molecular characteristics, reproducible growth, and relevance to alveolar epithelial tumours (Giard et al., 1973; Swain et al,.2010). Although chemotherapy continues to be a fundamental component for lung cancer management, the effectiveness of standard drugs is often compromised by poor tumour selectivity, quick systemic clearance, and major off-target toxicity (Zhu et al., 2021; Patel et al.,2024). These limitations highlight the urgent need for targeted drug delivery systems capable of enhancing intracellular drug accumulation in cancer cells while sparing normal tissues.

5-FU is a commonly used chemotherapeutic drug, and it has been shown to be effective against various solid tumours, such as lung, colorectal, and breast cancers (Zhong et al., 2025). The cytotoxic effects of 5-FU are primarily attributable to its inhibition of thymidylate synthase, alongside its misincorporation into RNA and DNA; these actions subsequently disrupt nucleic acid synthesis and trigger apoptosis (Longley et al., 2003). However, the clinical utility of 5-FU is hindered by its short plasma half-life, non-specific bio distribution, and dose-limiting systemic toxicity (Entezar-Almahdi et al., 2020). These drawbacks have motivated the development of carrier-based formulations that can improve drug stability, regulate release, and enhance tumour-specific delivery.

Nanotechnology provides adaptable platforms to address these issues by allowing the design of multifunctional nanocarriers with engineered physical, chemical, and biological properties. Of these, $Fe_2O_3$ NPs have attracted considerable attention for biomedical applications because of their biocompatibility, chemical inertness, large surface area, and ease of surface modification (Shestovskaya et al., 2023; Siciliano et al., 2022). $Fe_2O_3$ NPs can be used as effective drug carriers and also offer the possibility of imaging and magnetic guidance (Shubhra et al., 2023). For active targeting to tumor cells, surface modification with targeted ligands is a common approach. FA is of special interest in this context, as folate receptors are known to be overexpressed in a variety of epithelial cancers, including lung adenocarcinoma, but are expressed at low levels in most normal tissues (Ahmadi et al., 2023; Ledermann et al., 2015). FA-targeted nanocarriers rely on receptor-mediated endocytosis to preferentially accumulate in cancer cells, thus enhancing therapeutic potency and minimizing systemic toxicity (Martín-Sabroso et al., 2021).

In the context of the present study, we designed a nanotherapeutic system based on $Fe_2O_3$ NPs for the delivery of the anticancer drug 5-FU to A549 lung cancer cells using FA as a carrier. The rationale behind the $Fe_2O_3$-AFA-5FU NC system involves the conjugation of 5-FU with AFA to form an AFA-5-FU complex, followed by the final conjugation on the $Fe_2O_3$ NPs. This hierarchical design integrates the anticancer activity of 5-FU, the receptor-targeting activity of folic acid, and the carrier activity of $Fe_2O_3$ NPs into a single platform. Specifically, $Fe_2O_3$ NPs are expected to enhance the delivery of the anticancer 5-FU drug into lung cancer cells while using the tumour-targeting activity of the FA conjugate. The synthesized NCs were characterized by UV-visible spectroscopy, FT-IR, and SEM. *In-vitro* anticancer potential was evaluated in A549 cells using MTT cytotoxicity, cell-cycle analysis, caspase-mediated apoptosis, and scratch migration assay. Overall, the $Fe_2O_3$-FA-5-FU NC is expected to enhance the anticancer activity against A549 cells. Specifically, the purpose of the presented study is to establish an efficient $Fe_2O_3$ nanoparticle system.

## 2. MATERIALS AND METHODS

### 2.1 Materials

Ferric chloride heptahydrate ($FeCl_3.7H_2O$), sodium carbonate ($Na_2CO_3$), 5-fluorouracil (5-FU), and folic acid were obtained from Sigma-Aldrich (Bangalore, India) and used without further purification. N-Hydroxysuccinimide (NHS), dicyclohexylcarbodiimide (DCC), dimethyl sulfoxide (DMSO), triethylamine (TEA), methanol, diethyl ether, and other analytical-grade reagents were purchased from HiMedia Laboratories (Bangalore, India).

### 2.2 Synthesis $Fe_2O_3$ Nanoparticles

An aqueous solution of Fe(III) salt (0.1 M $FeCl_3{\cdot}7H_2O$) was hydrolysed by the addition of sodium carbonate (0.1 M $Na_2CO_3$) at a base-to-iron molar ratio of 2 ($OH^-/Fe^{3+}$). The hydrolysis reaction mixture was aged at 80 °C overnight to obtain iron polyoxocations, which resulted in the precipitation of goethite (α-FeOOH). The precipitate was filtered, washed, oven-dried, and then calcined at 400°C for 24 h in air to produce $Fe_2O_3$ NPs.

### 2.3 Activation of Folic Acid and its conjugation with 5-FU

The activation of FA was carried out by using previously reported methods (Liu et al., 2016). Briefly, FA (0.884 g) was dissolved in 20 mL of DMSO with a sonicator until a clear dilution was obtained. To this solution, DCC (0.784 g) and NHS (0.256 g) were added sequentially, followed by the addition of TEA (1 mL) for the activation of the carboxyl group in folic acid, and the reaction mixture was stirred at room temperature for 24 h under dark conditions. The obtained solid was washed with 30% acetone in diethyl ether (ice-cold) to get AFA. The product was dried and further used for conjugation with 5-FU.

AFA and 5-FU, each at 0.1 g, were dissolved in 20 mL of milli-Q water and allowed to react for 24 hours at room temperature with constant stirring. After that, the reaction mixture was then centrifuged at 5000 rpm for 30 minutes. The pellet, which contained conjugate, was then purified using dialysis with a 3.5 kDa molecular weight cut-off membrane. This dialysis lasted 6 hrs, with the Milli-Q water being replaced every hour. The post-dialysis sample was centrifuged and vacuum-dried at 40°C for 24 hours to get the AFA-5FU conjugate.

### 2.4 Surface functionalization of AFA-5FU onto $Fe_2O_3$ Nanoparticles

$Fe_2O_3$ NPs (25 mg) and AFA-5FU conjugate (25 mg) were dispersed in 10 mL of Milli-Q water using a sonicator and magnetically stirred for 2 hrs. To facilitate surface functionalization, the reaction mixture was kept for incubation in a rotary shaker at 200 rpm for 24 hrs. After the incubation process, the mixture was centrifuged at 8000 rpm for 20 min to collect the $Fe_2O_3$-AFA-5FU NCs. The pellet was washed repeatedly with Milli-Q water to remove any unbound conjugate. Subsequently, lyophilized for 48 hrs to obtain the product $Fe_2O_3$-AFA-5FU NCs and stored for further use.

### 2.5 Characterization of $Fe_2O_3$-AFA-5FU and $Fe_2O_3$ Nanoparticles

The UV-visible absorption spectrophotometer was employed to take spectra of 5-FU, bare $Fe_2O_3$ NPs, AFA, AFA-5FU conjugate, and $Fe_2O_3$-AFA-5FU NCs, and they were obtained within the wavelength range 200-800 nm. All samples were prepared by dispersing them in Milli-Q water, and they were measured in a quartz cuvette with a 1 cm optical path length, using Milli-Q water as the blank reference.

Fourier transform infrared (FTIR) spectroscopy was employed to detect functional groups and verify the conjugation process. Samples were dried and finely ground into fine powder along with potassium bromide (KBr) and pressed into pellets. Spectra were collected over the range of 4000-400 $cm^{-1}$ with background correction performed using pure KBr.

The surface morphology and particle size of the samples were examined by scanning electron microscopy (SEM) and ImageJ software, respectively. Prior to imaging, samples were mounted on carbon tape and sputter-coated with a thin conductive layer. SEM images were acquired under high-vacuum conditions, and particle size distribution was determined using ImageJ software based on Feret diameter measurements.

### 2.6 In-vitro Biological Activity

#### 2.6.1 Cell culture

Human adenocarcinoma (A549) cells and human embryonic kidney (HEK293) cells were obtained from the National Centre for Cell Science (NCCS), Pune, India. The cells were cultured in a culture flask containing DMEM/F12 medium (Gibco, USA) with 10% heat-inactivated fetal bovine serum (FBS), 1% penicillin–streptomycin (100 U/mL penicillin and 100 µg/mL streptomycin), and 1% L-glutamine. Cultured cells were incubated at 37°C in a humidified incubator with 5% $CO_2$. The culture media was replaced every 2–3 days, and cells were subcultured upon reaching approximately 80% confluency using 0.25% trypsin–EDTA. Cell morphology and

microbiological contamination were evaluated periodically.

### 2.6.2 Cytotoxicity Evaluation by MTT Assay

The cytotoxic effect of $Fe_2O_3$ NPs before and after their conjugation and 5-FU was evaluated by colorimetric MTT assay as follows (Mosmann et al., 1983). This is based on the mitochondrial enzyme-mediated conversion of pale yellow MTT to violet formazan crystals, which is measured in a spectrophotometer. The cultured cells (1 × $10^4$ cells/well) were placed in 96 flat-bottom well plates. Then these cells were exposed to different concentrations of prepared nanomaterials with tenfold dilution (1–100 µg/mL) and incubated at 37°C for about 48 hrs in a 5% $CO_2$ atmosphere. After 24 hrs of incubation, MTT reagent (5 mg/mL in PBS; 10 µL/well) was added and incubated for 4 h. Thereafter, the formazan crystals were dissolved in 200 µl of DMSO, and the absorbance was monitored using a microplate reader at a wavelength of 570 nm. The MTT assay was performed in parallel on normal HEK293 cells under identical experimental conditions to evaluate the cytocompatibility of the formulations.

$$\%\ \boldsymbol{Cell\ viabilty} = \left(\frac{\boldsymbol{Absorbance\ (Test-Blank)}}{\boldsymbol{Absorbance\ (Control-Blank)}}\right) \times \mathbf{100} \quad \textbf{(1)}$$

### 2.6.3 Flow Cytometric Analysis of Cell-Cycle Distribution

As previously reported (Kalejta et al., 1997), flow cytometry analysis was carried out in A549 cells cultured under standard conditions and exposed to $Fe_2O_3$-AFA-5FU NCs at their $IC_{50}$ concentration, while vehicle-treated cells were used as the control. After treatment, cells were collected, fixed in 70% ethanol, and stained with propidium iodide following RNase treatment to remove RNA interference. Cell-cycle distribution was determined based on fluorescence intensity using a BD FACS Calibur flow cytometer, and data acquisition was performed with BD Cell Quest Pro software (version 6.0) compared with control cells.

### 2.6.4 Quantification of Caspase-3, -8, and -9 Activities

The activity of Caspase 3, 8, and 9 in $Fe_2O_3$-AFA-5FU and the control was determined using a commercially available colorimetric assay kit in accordance with the manufacturer's instructions. Cells were grown in multi-well plates and treated with $Fe_2O_3$-AFA-5FU NCs at $IC_{25}$, $IC_{50}$, and $IC_{100}$ concentrations for 24 h, while control cells were treated with PBS buffer. After treatment, cells were washed, harvested, lysed, and supernatant was treated with Ac-DEVD-pNA, Ac-IETD-pNA, and Ac-LEHD-pNA (Casp-3, 8, and 9 assay kit, Sigma-Aldrich, USA). Finally, the optical density of supernatant samples was measured at 405 nm and quantified relative to control cells.

### 2.6.5 Assessment of Cell Migration by Wound-Healing Assay

Cell migration plays a major role in tumor progression and metastasis. The impact of $Fe_2O_4$-AFA-5FU NC and 5FU on cell migration was assessed by using a wound healing assay (Jonkman et al., 2014). The cells were seeded into six-well plates and allowed to grow until a confluent monolayer was formed. A scratch was created in the cell monolayer using a sterile 50 µL pipette tip. After removing detached cells by gentle washing with PBS, the cells were treated with control, 5-FU, and $Fe_2O_3$-AFA-5FU ($IC_{50}$) and incubated. The images of the wound were captured from the beginning of the wound till closure in the case of control with an interval of 6 hrs using an inverted microscope. The degree of wound closure was quantified using ImageJ software (version 1.54p), and cell migration was expressed as the percentage of wound closure calculated using Eq. (2).

$$\boldsymbol{Wound\ Closure}\ (\%) = \frac{(\boldsymbol{A_0 - A_t})}{\boldsymbol{A_0}} \times \mathbf{100} \quad \textbf{(2)}$$

Where, A0 denotes the wound area measured at 0 h and At represents the wound area at the corresponding time point

### 2.7 Statistical Analysis

All experiments were performed in triplicate. Data are expressed as mean ± standard deviation. Statistical analyses were conducted using GraphPad Prism version 10.1.0 (GraphPad Software, San Diego, CA, USA). Differences between groups were analyzed using one-way or two-way ANOVA followed by Tukey's post hoc test, Dunnett's test with respect to the control group, and also nonlinear regression, with $p < 0.05$ considered statistically significant.

## 3. RESULTS

### 3.1 Confirmation of $Fe_2O_3$ Nanoparticle Formation and Conjugation

The hydrolysis of $Fe^{3+}$ ions, when combined with sodium carbonate, yields the iron polyoxocations, which, upon aging at 80°C, precipitate as goethite (α-FeOOH). Calcination of the dried goethite at 400°C caused its phase transformation to crystalline α-$Fe_2O_3$ NPs through dehydration. This synthetic approach allows for precise control of phase evolution and results in α-$Fe_2O_3$ NPs, which are suitable for subsequent functionalization.

Successful synthesis and surface functionalization were confirmed by UV-vis and FTIR analyses. Spectral images showed characteristic iron oxide features and the appearance of functional group bands associated with folic acid activation and 5-FU conjugation, indicating effective surface modification. SEM micrographs showed uniformly distributed nanoscale particles with minimal agglomeration.

### 3.2 Characterization of $Fe_2O_3$-AFA-5FU Nanoconjugate

Figure 1 shows the UV–visible spectra of 5-FU, AFA, AFA-5FU conjugate, $Fe_2O_3$ NPs, and $Fe_2O_3$-AFA-5FUNCs. 5-FU had a UV absorption band that was typical of π–π* transitions, while AFA had a broad aromatic absorption (Chinnathambi et al., 2016). The AFA-5FU conjugate displayed merged spectral features with enhanced intensity, confirming successful conjugation. The $Fe_2O_3$ NPs showed weak, broad absorption (Meza et al., 2025), whereas AFA-5FU-$Fe_2O_3$ NCs exhibited increased absorbance and

spectral broadening with superimposed features of AFA and 5-FU, indicating successful surface functionalization and formation of a stable targeted NCs.

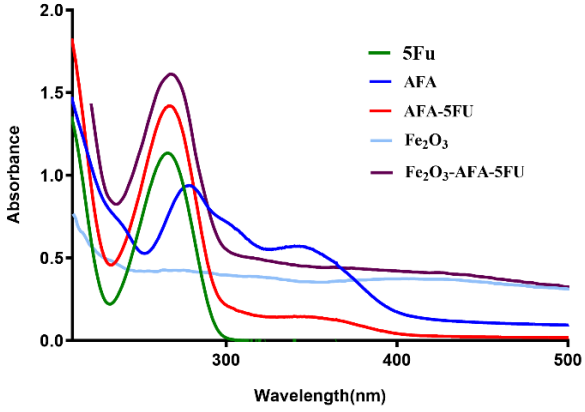


**Figure 1.** UV-Visible absorption spectra of 5-FU, AFA, AFA-5FU conjugate, $Fe_2O_3$ NPs, and $Fe_2O_3$-AFA-5FU NCs.

Figure 2 shows the FTIR spectra of $Fe_2O_3$ NPs, AFA, 5-FU, the AFA-5FU conjugate, and $Fe_2O_3$-AFA-5FU NCs. $Fe_2O_3$ NPs carried a strong absorption band (Begum et al., 2025) in the lower wavenumber region (~530–560 $cm^{-1}$), which is characteristic of Fe-O stretching vibrations and confirms the formation of iron oxide. The spectrum of AFA displayed prominent bands in the 3200–3500 $cm^{-1}$ region corresponding to -NH and -OH stretching, along with characteristic C=O and C-N vibrations in the region associated with characteristic molecular vibrations.5-FU displayed distinct absorption bands associated with carbonyl (C=O), C-F, and heterocyclic ring vibrations (Cheralayikkal et al., 2022). The AFA-5FU conjugate retained the main functional group bands of both components. However, noticeable shifts in the carbonyl and amide regions indicate successful chemical interaction between folic acid and 5-FU. The $Fe_2O_3$-AFA-5FU NCs showed the expected Fe-O vibration, thereby confirming preservation of the iron oxide core. AFA and 5-FU-corresponding absorption bands were also detected, including C=O vibrations and -NH/-OH stretching, but with minor changes and reduced intensity. These spectral shifts suggest surface binding and intermolecular interactions between the nanoparticle and the AFA-5FU conjugate, confirming successful functionalization and drug loading onto the $Fe_2O_3$ NPs.

SEM images (Figure 3(A)) showed that the synthesized $Fe_2O_3$ NPs mostly had a rod-like structure with minor morphological irregularities and moderate agglomeration, which is commonly observed for iron oxide nanostructures synthesized via wet-chemical methods. The nanorods were randomly oriented, and individual particles were clearly resolved in high-magnification images, allowing reliable size quantification.

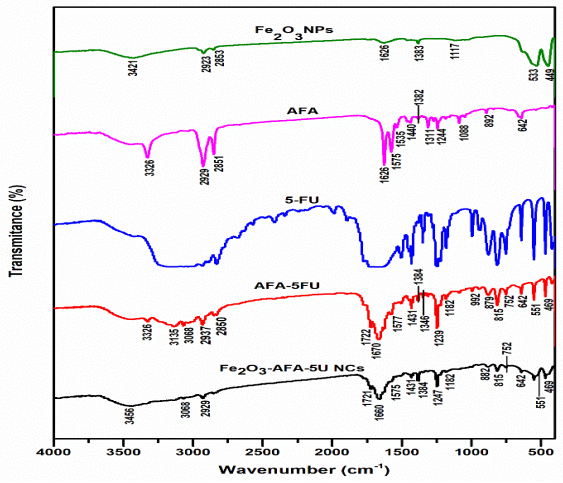


**Figure 2**. FTIR spectra of $Fe_2O_3$ NPs, AFA, 5FU, AFA-5FU conjugate, and $Fe_2O_3$-AFA-5FU $_4$ NCs, illustrating functional group interactions and confirming successful surface functionalization.

ImageJ software was used to analyze particle size and revealed the average Feret diameter of 43.45 ± 29.00 nm, with particle sizes ranging from 14 to 178 nm (n = 315). The size distribution histogram (Figure 3(B)) showed that most of the particles were between 20 and 50 nm in size, with a gradual extension toward larger sizes. This is because rod-shaped NPs naturally have different sizes. Overall, the distribution indicates a moderately polydisperse system, which is typical for anisotropic iron oxide nanomaterials.

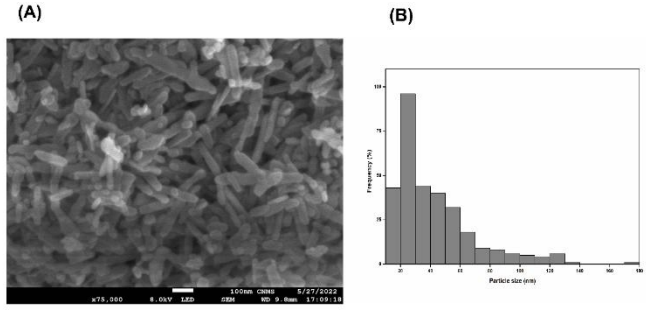


**Figure 3.** (A) SEM micrograph of $Fe_2O_3$ NPs showing predominantly rod-shaped morphology with moderate agglomeration. (B) Corresponding particle size distribution histogram derived from ImageJ analysis of SEM images (n = 315), illustrating the Feret diameter distribution and polydispersity of the nanostructures.

### 3.3 MTT-Based Cytotoxicity Analysis

The cytotoxic effects of 5-FU, $Fe_2O_3$ NPs, and $Fe_2O_3$-AFA-5FU NCs were evaluated by MTT assay (Figure 4(A)). Control cells maintained high viability, while 5-FU induced a concentration-dependent decrease in cell viability. $Fe_2O_3$ NPs showed minimal cytotoxicity near to the control group even at the highest concentration tested, indicating good biocompatibility. In contrast, $Fe_2O_3$-AFA-5FU NCs showed a greater reduction in cell viability than 5-FU, demonstrating enhanced antiproliferative activity. The percentage inhibition profile (Figure. 4(B)) further confirmed the superior cytotoxic efficacy of the NCs, likely due to folic acid–mediated cellular uptake and improved drug delivery, which is also further supported by the $IC_{50}$ values (Table 1). The $Fe_2O_3$ NPs,

$Fe_2O_3$-AFA-5FU NCs exhibited negligible cytotoxicity toward HEK293 normal cells (Figure. 4(C)), maintaining >90% viability across all tested concentrations, indicating good biocompatibility.

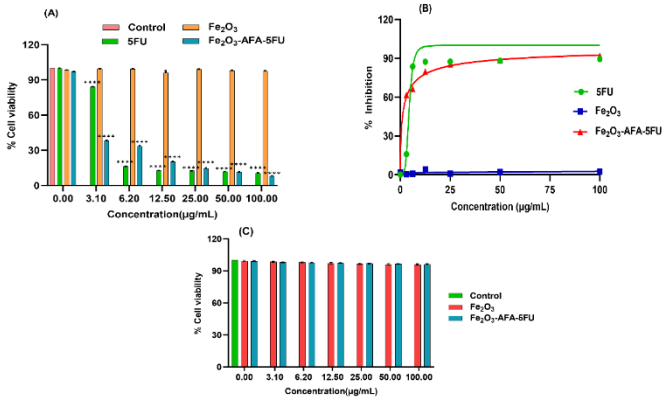


**Figure 4.** Effect of 5-FU, $Fe_2O_3$ NPs, and $Fe_2O_3$-AFA-5FU NCs on cell viability in A549 cells and HEK293 cells. (A) Percentage cell viability of A549 cells determined by MTT assay following treatment with increasing concentrations of 5-FU, $Fe_2O_3$ NPs, and $Fe_2O_3$-AFA-5FU NCs. (B) Corresponding dose-response curves showing percentage inhibition used for $IC_{50}$ determination in A549 cells. (C) Cytotoxicity evaluation in HEK293 cells demonstrating the biocompatibility of $Fe_2O_3$ NPs and $Fe_2O_3$-AFA-5FU NCs toward normal cells.

**Table 1. $IC_{50}$ values determined by MTT assay**

| Treatment | $IC_{50}$ (µg/mL) |
|---|---|
| 5-FU | 4.423 |
| $Fe_2O_3$ NPs | Not Determined |
| $Fe_2O_3$-AFA-5FU NCs | 1.546 |

### 3.4 Effect of Treatment on Cell-Cycle Distribution

The cell-cycle distribution was examined to see how the $Fe_2O_3$-AFA-5FU NCs affected the cell cycle progression, as shown in Figure 5. The control cells had a normal cell cycle distribution, with the predominance of cells in the $G_0/G_1$ phase, followed by the S and $G_2$/M phases. Conversely, the cells treated with $Fe_2O_3$-AFA-5FU NCs displayed a marked shift in the cell cycle distribution. There was a considerable elevation in the sub-$G_0/G_1$ phase, which indicated apoptotic cell death due to the treatment. Moreover, there was a significant reduction in the $G_0/G_1$ phase, with cells accumulating in the $G_2$/M phase, which indicated that the cells were arrested at this stage of the cell cycle. Statistical analysis confirmed that the results were significantly different from those of the control group ($p < 0.05$).

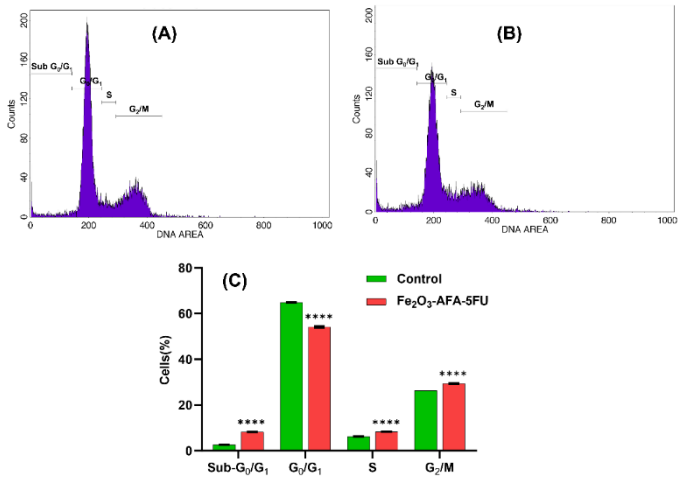


**Figure 5**. Cell-cycle analysis of A549 cells following $Fe_2O_3$-AFA-5FU NCs treatment. (A) Representative propidium iodide (PI) fluorescence histogram of untreated A54 9 cells. (B) PI histogram of A549 cells treated with AFA-5FU-$Fe_2O_3$ NCs for 24 h.(C) Quantitative distribution of cells in sub-$G_0/G_1$, $G_0/G_1$, S, and $G_2$/M phases following treatment. Data are presented as mean ± SD (n = 3).

### 3.5 Caspase-Mediated Apoptotic Activation

Caspase activity assays were carried out to understand the mechanism of apoptosis triggered by $Fe_2O_3$-AFA-5FU NCs (Figure 6). The treatment caused a substantial and concentration-dependent increase in the activities of caspase-3, caspase-8, and caspase-9 compared to the control cells. It is pertinent to note that the marked activation of both initiator caspases (caspase-8 and caspase-9) and the substantial increase in the activity of the executioner caspase-3 indicate the activation of both extrinsic and intrinsic pathways of apoptosis. These results clearly confirm that $Fe_2O_3$-AFA-5FU NCs are effective in triggering apoptosis in a dose-dependent manner and also statistically significant ($p < 0.05$).

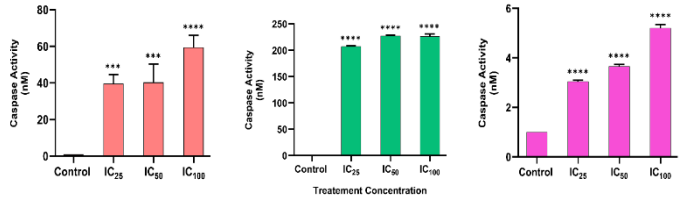


**Figure 6**. Caspase activation in A549 cells following treatment with $Fe_2O_3$-AFA-5FU NCs. (A) Caspase-3, (B) caspase-8, and (C) caspase-9 activities measured after exposure to $IC_{25}$, $IC_{50}$, and $IC_{100}$ concentrations. Data are presented as mean ± SD (n = 3). Statistical significance was determined using one-way ANOVA, with ***$p < 0.001$ and ****$p < 0.0001$ compared to control.

### 3.6 Effect on Cell Migration

The impact of $Fe_2O_3$-AFA-5FU NCs on cell migratory behavior was investigated using a wound-healing assay. As shown in Figure 7(A), control cells showed rapid wound closure over a period, with near-complete closure observed at 30 h. Cells treated with 5-FU showed a moderate reduction in migration, as indicated by delayed wound closure

compared to the control group. In contrast, treatment with $Fe_2O_3$-AFA-5FU NCs markedly inhibited cell migration, with a substantial portion of the wound area remaining open even after 30 h.

Quantitative analysis of percentage wound closure (Figure 7(B)) demonstrated a time-dependent increase in migration for all groups; however, the extent of wound closure was significantly lower in the $Fe_2O_3$-AFA-5FU-treated cells at all time points compared with both control and 5-FU-treated cells ($p < 0.05$). These findings indicate that $Fe_2O_3$-AFA-FU NCs effectively suppress cell migration, suggesting a strong anti-migratory potential in addition to their cytotoxic effects.

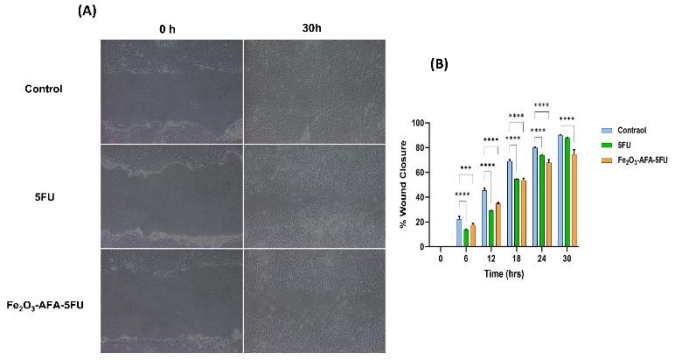


**Figure 7.** (A) Representative phase-contrast images of the wound-healing assay showing cell migration in control, 5-FU, and $Fe_2O_3$-AFA-5FU NCs treated cells at 0 h and 30 h. (B) Quantitative analysis of wound closure expressed as percentage over time. Data are presented as mean ± SD (n = 3). Statistical significance was determined using two-way ANOVA followed by Tukey's multiple comparison test; significance is indicated at selected time points for clarity (****$p < 0.0001$ vs. control). Scale bar: 100 µm.

## 4. DISCUSSION

In the current work, $Fe_2O_3$-AFA-5FU NCs were successfully prepared using a stepwise approach that included the controlled formation of $Fe_2O_3$ NPs, carbodiimide-induced activation of folic acid, conjugation with 5-FU, and subsequent surface functionalization on the surface of $Fe_2O_3$ NPs. The synthesis technique ensured the formation of a stable $Fe_2O_3$ core while enabling efficient drug conjugation and folate-mediated targeting.

The Fe(III) precursors were hydrolysed, and subsequent aging facilitated the synthesis of goethite, which upon calcination yielded the $Fe_2O_3$ NPs. This tuned precipitation–calcination process technique is a well-established method for the production of phase-pure iron oxide with a favorable surface for functionalization. SEM analysis discovered that $Fe_2O_3$ NPs were primarily rod-shaped with moderate agglomeration and a moderately polydisperse size distribution, which is characteristic for anisotropic iron oxide nanostructures synthesized via wet-chemical methods. The nanoscale dimensions and exposed surface area of $Fe_2O_3$ NPs provide a favorable platform for drug conjugation and cellular interaction.

UV-visible and FTIR spectra revealed that folic acid was successfully activated and conjugated with 5-FU. UV-visible spectroscopy displayed the characteristic absorption peaks of both AFA and 5-FU in the AFA-5FU conjugate, indicating molecular interaction. The $Fe_2O_3$-AFA-5FU NCs displayed higher absorbance and spectral broadening, which signify changes in the local electronic environment due to surface binding. FTIR spectra also justified the conjugation by the presence of Fe-O vibrations, in addition to organic functional group bands ascribed to AFA and 5-FU, accompanied by minor shifts and decreased intensities, which are characteristic of the nature of intermolecular interactions and successful surface functionalization.

The biological analysis revealed that the $Fe_2O_3$ NPs showed minimal cytotoxicity, thus proving their biocompatibility. However, the $Fe_2O_3$-AFA-5FU NCs had higher concentration-dependent cytotoxicity than the 5-FU, as revealed by the MTT assay. This could be due to the folate-mediated uptake of the NCs by folate receptor overexpressing cells and improved intracellular delivery of 5FU, thus providing an advantage of targeted delivery of the NCs over the drug alone. Furthermore, the minimal reduction in HEK293 cell viability across the concentrations suggests a favorable cytocompatibility profile with respect to normal cells. In contrast to the pronounced cytotoxic response observed in A549 cancer cells, the limited effect on HEK293 cells suggests enhanced therapeutic selectivity, likely resulting from differential folate receptor expression and cellular internalization pathways between malignant and non-malignant cells.

The cell cycle analysis revealed that $Fe_2O_3$-AFA-5FU NCs induced a significant disruption of the normal cell cycle. A notable elevation in the sub-$G_0/G_1$ phase was observed, along with an accumulation of cells within the $G_2$/M phase, thereby suggesting both apoptosis and cell cycle arrest. These results suggest that the NCs interfere with the DNA synthesis and mitosis, thereby impeding cell proliferation.

The apoptotic mechanism behind the cytotoxic effect was further investigated using caspase activity assays. The significant and dose-dependent activation of initiator caspases-8 and -9 revealed that both the extrinsic and intrinsic pathways of apoptosis were involved. The concurrent increase in executioner caspase-3 confirmed that these pathways were merged and programmed cell death was implemented. These results collectively show that $Fe_2O_3$-AFA-5FU NCs induce apoptosis through multiple signaling pathways, thereby increasing their anticancer efficacy.

In addition to the cytotoxic and apoptotic activities, the wound healing assay also showed a strong inhibition of cell migration by the $Fe_2O_3$-AFA-5FU NCs. Compared with control and 5-FU-treated cells, NC-treated cells demonstrated considerably decreased wound closure over the experimental period, indicating strong anti-migratory potential. This anti-migratory activity is especially important in the context of cancer progression, as it indicates the ability of the NCs to suppress the processes associated with tumor invasion and metastasis.

In summary, the combination of physicochemical characterization and *in-vitro* biological studies clearly shows that $Fe_2O_3$-AFA-5FU NCs have improved anticancer efficacy

due to targeted delivery, apoptosis induction, cell cycle arrest, and inhibition of cell migration.

## 5. CONCLUSION

In conclusion, the $Fe_2O_3$-AFA-5FU NCs were successfully synthesized and characterized, thereby validating the effective folic acid–mediated drug conjugation and their surface functionalization on the $Fe_2O_3$ NPs. These NCs showed improved anticancer efficacy compared to 5-FU, while preserving the iron oxide core's cell compatibility. Enhanced cytotoxicity was facilitated by targeted cellular uptake, leading to cell-cycle arrest, the activation of both intrinsic and extrinsic apoptotic pathways, and a significant reduction in cell migration. Consequently, these results demonstrate the potential of $Fe_2O_3$-AFA-5FU NCs as a promising targeted drug delivery system for anticancer therapy. Further in vivo investigations are necessary to confirm their therapeutic efficacy and safety profile.

## DISCLOSURE

Funding: None.

## CONFLICT OF INTEREST

The authors declare no conflict of interest.

## ACKNOWLEDGEMENTS

The authors gratefully acknowledge the Department of Science and Technology (DST), Government of India, for providing the instrumentation facilities established at the Department of Biochemistry, Kuvempu University, Shankaraghatta, Karnataka, under the Fund for Improvement of Science and Technology (FIST) scheme (Grant No. SR/FST/LS-1/2018/175(C)), which were utilized to carry out this study.

## REFERENCES


1. Ahmadi M, Ritter CA, von Woedtke T, Bekeschus S, Wende K. Package delivered: folate receptor-mediated transporters in cancer therapy and diagnosis. Chemical Science. 2024;15(6):1966-2006.
2. Begum SK, Shabnam D, Haque N, Alam MJ, Ferdous J, Nur UJ, Fatema K, Shabiha RJ, Clarke RJ, Chowdhury P, Uddin MN. Green synthesis of magnetite (Fe3O4) and hematite (Fe2O3) nanoparticles using Moringa oleifera and Psidium guajava leaf extracts for sustainable applications. Scientific Reports. 2025 Oct 17;15(1):36465.
3. Cheralayikkal S, Manoj K, Hussan KS. Formulation and evaluation of a smart drug delivery system of 5-fluorouracil for pH-sensitive chemotherapy. Heliyon. 2022 Jul 1;8(7).
4. Chinnathambi S, Karthikeyan S, Kesherwani M, Velmurugan D, Hanagata N. Underlying the mechanism of 5-fluorouracil and human serum albumin interaction: a biophysical study. J. Phys. Chem. Biophys. 2016;6(2):100021410-4172.
5. Entezar-Almahdi E, Mohammadi-Samani S, Tayebi L, Farjadian F. Recent advances in designing 5-fluorouracil delivery systems: a stepping stone in the safe treatment of colorectal cancer. International journal of nanomedicine. 2020 Jul 30:5445-58.
6. Giard DJ, Aaronson SA, Todaro GJ, Arnstein P, Kersey JH, Dosik H, Parks WP. In vitro cultivation of human tumors: establishment of cell lines derived from a series of solid tumors. Journal of the National Cancer Institute. 1973 Nov 1;51(5):1417-23.
7. Jonkman JE, Cathcart JA, Xu F, Bartolini ME, Amon JE, Stevens KM, Colarusso P. An introduction to the wound healing assay using live-cell microscopy. Cell adhesion & migration. 2014 Sep 3;8(5):440-51.
8. Kalejta RF, Shenk T, Beavis AJ. Use of a membrane-localized green fluorescent protein allows simultaneous identification of transfected cells and cell cycle analysis by flow cytometry. Cytometry: The Journal of the International Society for Analytical Cytology. 1997 Dec 1;29(4):286-91.
9. Ledermann JA, Canevari S, Thigpen T. Targeting the folate receptor: diagnostic and therapeutic approaches to personalize cancer treatments. Annals of Oncology. 2015 Oct 1;26(10):2034-43.
10. Liu W, Nie L, Li F, Aguilar ZP, Xu H, Xiong Y, Fu F, Xu H. Folic acid conjugated magnetic iron oxide nanoparticles for nondestructive separation and detection of ovarian cancer cells from whole blood. Biomaterials science. 2016;4(1):159-66.
11. Longley DB, Harkin DP, Johnston PG. 5-fluorouracil: mechanisms of action and clinical strategies. Nature reviews cancer. 2003 May 1;3(5):330-8.
12. Martín-Sabroso C, Torres-Suárez AI, Alonso-González M, Fernández-Carballido A, Fraguas-Sánchez AI. Active targeted nanoformulations via folate receptors: State of the art and future perspectives. Pharmaceutics. 2021 Dec 22;14(1):14.
13. Meza Ramírez EA, Pérez Centeno A, Campos-González E, Camps E, Quiñones Galván JG. Synthesis and characterization of $Fe_2O_3$ nanoparticles via pulsed laser ablation in liquids: effects of solvent and laser fluence. Scientific Reports. 2025 Oct 21;15(1):36641.
14. Molina JR, Yang P, Cassivi SD, Schild SE, Adjei AA. Non-small cell lung cancer: epidemiology, risk factors, treatment, and survivorship. InMayo clinic proceedings 2008 May 1 (Vol. 83, No. 5, pp. 584-594). Elsevier.Giard, D. J. et al. *J. Natl. Cancer Inst.* **1973**, *51*, 1417–1423.
15. Mosmann T. Rapid colorimetric assay for cellular growth and survival: application to proliferation and cytotoxicity assays. Journal of immunological methods. 1983 Dec 16;65(1-2):55-63.
16. Patel P, Raval M, Airao V, Ali N, Shazly GA, Khan R, Prajapati B. Formulation of folate receptor-targeted silibinin-loaded inhalable chitosan nanoparticles by the QbD approach for lung cancer targeted delivery.

ACS omega. 2024 Feb 24;9(9):10353-70.
17. Shestovskaya MV, Luss AL, Bezborodova OA, Makarov VV, Keskinov AA. Iron oxide nanoparticles in cancer treatment: cell responses and the potency to improve radiosensitivity. Pharmaceutics. 2023 Sep 30;15(10):2406.
18. Shubhra QT. Iron oxide nanoparticles in magnetic drug targeting and ferroptosis-based cancer therapy. Medical Review. 2023 Oct 26;3(5):444-7.
19. Siciliano G, Monteduro AG, Turco A, Primiceri E, Rizzato S, Depalo N, Curri ML, Maruccio G. Polydopamine-coated magnetic iron oxide nanoparticles: from design to applications. Nanomaterials. 2022 Mar 30;12(7):1145.
20. Swain RJ, Kemp SJ, Goldstraw P, Tetley TD, Stevens MM. Assessment of cell line models of primary human cells by Raman spectral phenotyping. Biophysical journal. 2010 Apr 21;98(8):1703-11.
21. Zhong C, Wang S, Jiang WJ, Li Z, Wang X, Fan S, Huang J, Wu HJ, Sheng R, Fei T. Chemoresistance mechanisms to 5-Fluorouracil and reversal strategies in lung and breast cancer. Scientific Reports. 2025 Feb 19;15(1):6074.
22. Zhu X, Yu Z, Feng L, Deng L, Fang Z, Liu Z, Li Y, Wu X, Qin L, Guo R, Zheng Y. Chitosan-based nanoparticle co-delivery of docetaxel and curcumin ameliorates anti-tumor chemoimmunotherapy in lung cancer. Carbohydrate polymers. 2021 Sep 15; 268:118237.